Structural and electronic characterisation of Cu/Au(111) near-surface alloys

Federico Grillo[1*], Rory Megginson[1], David Batchelor[2*], Matthias Muntwiler[3*], and Christopher J. Baddeley[1]

[1]*EaStCHEM – School of Chemistry, University of St. Andrews, St. Andrews, KY16 9ST, United Kingdom*

[2] *Karlsruhe Institut für Technologie (KIT) - IPS, Hermann-von-Helmholtz-Platz 1, 76344 Eggenstein, Deutschland*

[3]*Paul Scherrer Institut, Laboratory for Micro- and Nanotechnology. WSLA/122, 5232 Villigen PSI, Switzerland*

E-mail: federico.grillo@st-andrews.ac.uk; david.batchelor@kit.edu; matthias.muntwiler@psi.ch

Geometrical structure and electronic characteristics of ultrathin metallic films of one metal on another are strongly influenced by factors such as lattice mismatch and formation of near-surface alloys. Doped systems often show modified chemical-physical properties which may be amenable to different reactivity routes. Copper-gold surface alloys have received the attention of several studies, only a few of which have been undertaken in an UHV environment, using surface sensitive techniques. In this contribution, systems produced upon room temperature deposition of copper on the (22×√3)-Au(111) surface, at various copper loadings and annealed to different temperatures, are investigated using scanning tunnelling microscopy and synchrotron radiation based techniques (X-ray photoelectron diffraction, photoemission), with comparison with some theoretical modelling. Overall the *fcc* lattice is essentially maintained on preparation. Upon thermal treatments structural and compositional changes, in favour of alloyed structures with tetragonal packing, are seen.

Keywords: X-ray Photoelectron Diffraction (XPD), Photoemission, Scanning Tunnelling Microscopy (STM), Synchrotron, Surface Alloys

1. Introduction

Binary metal alloys have been the subject of much investigation,[1, 2] owing to their widespread use in several fields spanning construction, transportation, electronics, medicine and chemistry. Often the physical properties of bulk alloys are regarded as a linear combination of the properties of the single components; in particular, the lattice parameter is described by Vegard's law.[3] Copper-gold alloys find application in a variety of diverse fields such as catalysis,[4] protection from corrosion[5] and jewellery.[6] The Cu/Au phase diagram shows that copper and gold are completely miscible over the whole range of concentrations and a large range of temperatures.[2, 7, 8] The alloy has a cubic unit cell, the bulk lattice parameter of which positively deviates from Vegard's law.[3] Only a few ordered phases are known:[9] for a one to one copper to gold stoichiometry, below *ca.* 700 K, two ordered phases exist. The AuCu I phase, type $L1_0$, has a tetragonal superstructure and is stable at low temperatures.[10] The second known stable phase is AuCu II, which differs from AuCu I in that it has nearly periodic antiphase boundaries along the *y*-axis of the unit cell, on average every five unit cells.[10] Other stable structures include Cu_3Au (type $L1_2$) and $CuAu_3$ (type $L1_2$), in decreasing order of stability.[7] Recently, scanning tunnelling microscopy (STM) investigations have focused on the surface layers of Cu/Au alloys,[11, 12, 13] prepared by annealing copper thin films deposited on Au(111) surfaces, highlighting the growth mode and how ordered surface terminations can be prepared.[13] The nucleation process of guest metals on Au(111) generally follows the place-exchange mechanism,[14] which was initially ruled out for the addition of copper; however, the same mechanism was later confirmed also for copper.[11]

Although the nucleation step of guest metals on Au(111) seems now well understood,[11, 12, 13, 14, 15, 16, 17, 18, 19, 20] the morphology and composition of the top layer are still a matter of debate. Specifically for the addition of copper, several studies report island growth without copper intermixing with the underlying gold,[21, 22, 23] while others report intermixing for every coverage even at room temperature.[24, 25] Complete encapsulation, whereby a single copper layer is covered by a single gold layer, has also been proposed.[12, 24, 25, 26] Further, it has been suggested that the structure and chemical composition of the layers below the first play an important role in dictating the reactivity of such surfaces,[5, 12, 13, 24, 26] most likely due to random intermixing between the two metals and chemically induced surface segregation phenomena. In order to rationalize the properties of such structures, it is crucial to characterize the layers just below the first, the top one having been successfully characterized via STM.[11, 12, 13] This requires the use of techniques which can gather precise

information on a larger area than that evaluated via STM, typically a few square nanometres, however, still maintaining sensitivity to the near surface layers.

In this contribution the top layers of structures prepared by depositing thin films of copper on Au(111) are investigated using STM and synchrotron radiation based techniques: X-ray photoelectron diffraction (XPD) allows one to access geometrical information on a larger scale than STM, albeit averaged; and photoemission spectroscopy (PES) is used to quantify elements and their chemical states, looking at both core level and valence band regions. Both techniques are not only sensitive to the surface, but also to the layers immediately below it.

Experimental results show structural and compositional changes upon annealing. The determination of the structure of the uppermost layers is not trivial. However, through the complementarity of the techniques employed, the overall geometry of the top layers is seen to change from *fcc*, for multilayers of copper on Au(111), to tetragonal, when the near surface alloys are formed.

2. Experimental methods

The original STM investigation was carried out at the University of St. Andrews[11, 13] and was used as a basis for the present work, which was undertaken at the PEARL (Photoemission and Atomic Resolution Laboratory) beamline at the Swiss Light Source (SLS).[27] The beamline houses a variety of surface science techniques together with synchrotron radiation methods allowing one to gather information on the surface and near-surface layers. Base pressures in analysis, probe, and preparation chambers were all *ca.* 1×10^{-10} mbar.

The Au(111) crystal was cleaned by cycles of argon ion sputtering and annealing to *ca.* 870 K until wide terraces characteristic of the typical Au(111)-($22\times\sqrt{3}$) surface reconstruction were observed via STM.[28, 29] Cleanliness after preparation of the Au(111) crystal was verified by photoemission spectroscopy. The clean Au 4f core level spectra showed the well-known low binding energy shifted surface component.[30] Copper deposition was achieved using a well outgassed FOCUS EFM evaporator and a 99.999% pure copper rod. During copper deposition the pressure increased to *ca*. 8×10^{-10} mbar. The copper deposition rate was *ca.* 0.02 ML min^{-1}. The coverage was calibrated collecting the Cu $2p_{3/2}$ core level photoemission signal from a clean Cu(110) crystal as reference, at a photon energy (PE) of 1045 eV, together with the evaluation of the attenuation of the Au 4f core level signal

recorded with a PE of 143 eV. Coverage evaluation is based on the assumption that the copper layer grows in a Frank-van der Merwe fashion[31] with no intermixing; a 1 ML coverage is defined as one copper atom per surface unit cell of Au(111). After preparation of the copper layer, the deposition was verified by photoemission spectroscopy. For surface sensitivity the PE for each of the core level transitions was chosen such as to obtain spectra at a kinetic energy of *ca.* 50 eV. The C 1s and O 1s spectra showed nothing above the noise, which, based on cross sections[32] and escape depths[33] at these kinetic energies, leads to upper limits of *ca.* 0.01 ML for both elements. Binding energy (BE) values are referred to the Fermi level collected at each PE. Various copper coverages were investigated from sub-monolayers to a few monolayers (*ca.* 2.7 ML). Analyser and beamline settings were chosen so that the detailed spectra were lifetime limited. The Cu 2p3/2 photoelectron diffraction data was collected over the complete 2π azimuth and a θ range up to 80° to the surface normal; details are reported in Ref.[27] The photoelectron diffraction modulation[34, 35, 36] data were extracted using a 3×3 point averaging with a simple constant background subtraction and integration over the peak.

3. Results and discussion

Following Ref.[13] the surface alloy was prepared by annealing a *ca.* 2.7 ML preparation to *ca.* 530 K. This process is represented schematically in figure 1. A copper layer *ca.* 2.7 ML thick is deposited on Au(111), figure 1(a); some interdiffusion already occurs, as a result of the nucleation mechanism following the place-exchange mechanism.[11, 13] For coverages above 1 ML, the top layers show a moiré structure.[12, 13, 26] The system is then annealed to promote atomic mobility and diffusion, figure 1(b); as an effect of the annealing, copper sinks into the bulk gold. The extent of alloying is controlled by the annealing time and temperature.

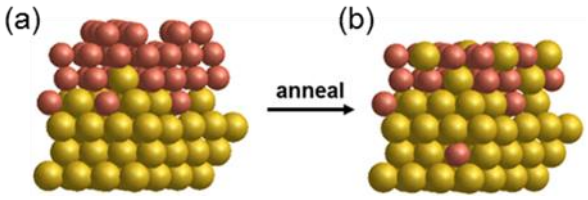

Fig. 1. Schematics of the process for creating the surface alloy: (a) *ca.* 3 ML of copper (dark orange) are added to Au(111) (yellow); (b) the system is then annealed to promote atoms interdiffusion.

In figure 2 STM images following preparation are reported. Figure 2(a) shows the moiré structure that forms for a copper coverage of 2 ML and above,[12, 13, 26] as a result of the interference between the added copper layers and Au(111) lattice. The appearance of a moiré pattern can be considered as an indication that only a small amount of intermixing between the two metals can occur. In principle the moiré pattern is generated by the lattice mismatch between the lattice unit cells of Cu(111), 0.256 nm, and Au(111), 0.288 nm. However, in the present case it is clear that considerable intermixing is occurring and that the moiré can also indicate the accommodation of the lattice space change from the surface layer (essentially copper) to the bulk (gold), going through a heavily alloyed interfacial region.

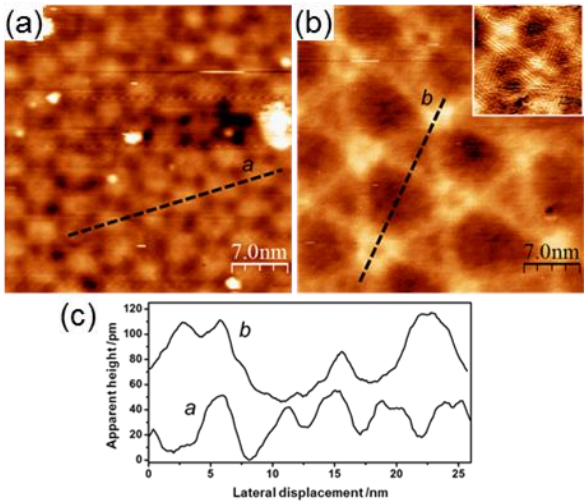

Fig. 2. STM images of the *ca.* 3 ML Cu/Au(111) before, (a), and after annealing, (b). (a) 35×35 nm^2, 0.6 nA, -1.1 V; (b) 35×35 nm^2, 0.7 nA, 1.1 V; inset 15×15 nm^2, 0.3 nA, 0.4 V; (c) line profiles as in (a) and (b).

For a coverage thicker than *ca.* 3 ML the system is reported to behave as a bulk copper {111} termination.[12, 26] The moiré has an average pseudo-periodicity of *ca.* 4.5 nm, as shown by the line profile *a* in figure 2(c). Upon annealing the surface alloy forms, figure 2(b); this is evidenced by surface features evolving into a different moiré structure having much larger, nearly double, average pseudo-periodicity, as shown by the line profile *b* in figure 2(c). The inset in figure 2(b) shows atomic resolution on the alloyed structure.

Figure 3 shows Cu 2p3/2 core level and valence band photoemission spectra collected choosing the photon energies so that the kinetic energy was similar, so that a similar depth from the surface layer is probed, ensuring the same surface sensitivity.

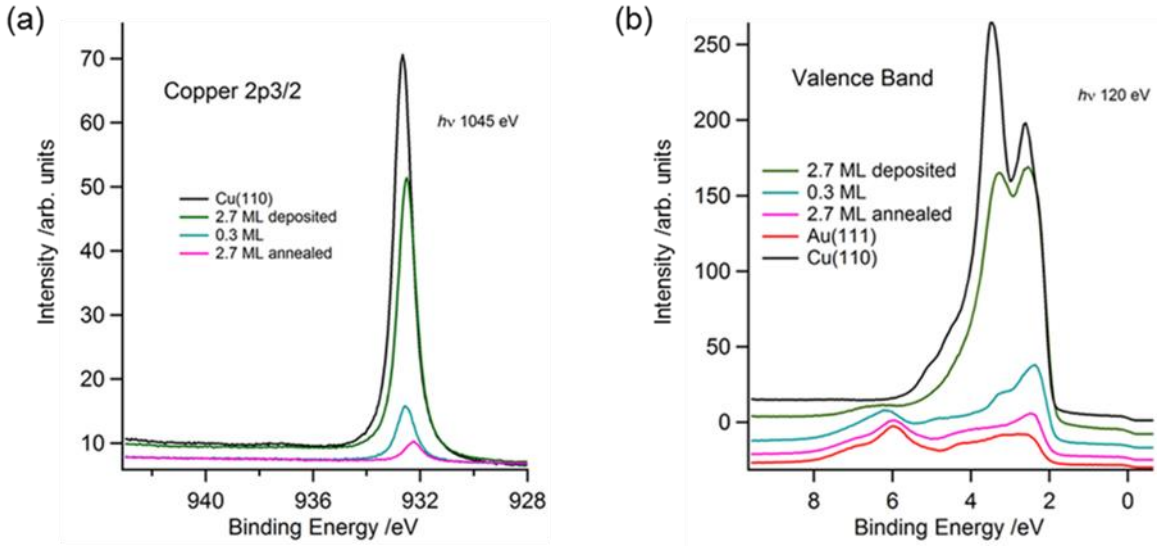

Fig. 3. Cu 2p3/2 photoemission (a) and valence band (b) spectra collected at copper increasing coverage (before annealing) and after annealing. Valence band spectra have been offset for clarity.

Figure 3(a) shows the Cu 2p3/2 core level spectra for three preparations together with that of a Cu(110) crystal. The quoted coverages are based on a simple quantification based on a layer-by-layer growth mode which, considering the STM observations[12, 13, 26] is clearly inappropriate to describe the growth process in full. Nevertheless, given the complexity of both nucleation and growth steps, this is a simple and prudent choice. On closer observation, there is a shift in the binding energy of the Cu 2p3/2 spectra from 932.1 eV at the lowest submonolayer coverage, to that of bulk copper, as measured on a clean Cu(110) single crystal, at 932.5 eV. At *ca.* 3 ML the BE value (932.4 eV) is very close to that of bulk copper. The overall peak shift across the range of coverages investigated is 0.4 eV, a much smaller value than its FWHM, *ca.* 0.85 eV, which remains constant. STM investigations[11, 12, 13, 26] show that the morphology of the top layers undergoes considerable changes and cannot be associated with the presence of a single metal. In particular for the low coverage regime (below *ca.* 1 ML), this indicates that there is a subsurface region which is rather rich in copper. The presence of a subsurface copper-rich layer for the Cu/Au system is in agreement with several computational studies.[37, 38, 39, 40] The layers above the first exhibit a moiré structure instead; also in these layers some intermixing is seen,[12, 26] however to a lesser extent than for the interfacial layer. At above *ca.* 3-4 ML, copper thin films exhibit electronic characteristics similar to those of bulk copper.[12, 26] This can be explained on the basis of the relative mobility of the atoms in the uppermost surface layers, when compared to that of the bulk-like layers underneath. As a consequence of such a variable degree of intermixing, different growth modes are experienced. In this case one might expect various copper species

to be identified by distinct binding energy shifts; however this is not observed. Such a shift was not observed by Zhao and co-workers,[24] likely because only the dissolution of 1 ML thick copper film into bulk gold was investigated. In such a system, the copper layer is sub-surface already after preparation and the different chemical environments that copper atoms experience when dissolving further into the bulk may be difficult to observe because of differences in escape depths and also the fact that a conventional non-monochromatic X-ray source was used compared to a monochromatized synchrotron source as at PEARL.

On the basis of previous experimental work, ion scattering and X-Ray Photoelectron Spectroscopy (XPS)[24] and STM,[11, 12, 13, 26, 41] it is clear that the copper is easily incorporated below the gold surface at room temperature even at sub-monolayer coverage. At higher copper coverages the two metals interdiffuse forming a copper rich subsurface region. The gold concentration in the copper layers is seen to decrease with increasing copper coverage (the thicker the copper layer, the lower the gold content). The diffusion of copper into the bulk gold is facilitated with increasing temperature. This is seen for the 2.7 ML coverage which, on annealing, decreases to a value which nominally corresponds to a *ca.* 0.1 ML, clearly demonstrating the dissolution of the copper into the gold bulk.

Figure 3(b) shows valence band measurements recorded for the same copper coverages as in figure 3(a) and that of a clean Au(111) sample. Here of interest is the relative signal intensity, when compared to that of the Cu 2p3/2 core level, and also the intensity of the copper and gold contributions to the valence band. The latter can be understood in terms of the relative size of the cross sections of the Cu 3d and Au 5d levels, 5.139 Mb and 0.4332 Mb at a PE of 132.3 eV, respectively.[32] The very intense valence band signal of the 2.7 ML copper preparation decreases by almost a factor of 50 on annealing; by comparison, the decrease in intensity of the Cu 2p3/2 is about a factor of 15. This is difficult to explain as the kinetic energies of the electrons are very similar (Cu 2p3/2 113 eV, valence band 117 eV) so the depth probed by the photoelectrons is similar. The reason for the different decrease in signal is probably due to alloying. The electronic structure of the bonding orbitals will change with alloy composition and consequently the valence band photoemission will change. Indeed, in all coverage regimes up to and including the 2.7 ML simple weighted sums are unable to explain the changes in the valence band, indicating complex growth is present over the whole range studied. This is also supported by the observed shifts in the Cu 2p3/2 core levels.

As discussed above, the growth and dissolution of copper in the Au(111) surface are complex processes and, as such, may occur following different mechanisms. However, with

a controlled annealing process, near surface alloy with an ordered structured can be formed. This is shown in figure 2(b) which shows the moiré that is formed on annealing.[13] A short range ordered structure is seen within the moiré, as highlighted in the inset in figure 2(b). The question now arises as to whether this is purely a local ordering on the uppermost surface layers or is connected to the bulk; in the latter case, what is the relation between the surface layer and the bulk. This is a difficult and complicated question and to gain an insight into this the synchrotron related technique of angle resolved XPD was chosen as both surface and signals from buried layers can be readily distinguished. Photoelectron diffraction is a well-established laboratory and synchrotron technique for structural analysis.[34, 35, 36, 42] It is also chemical element and state sensitive from the choice of the photoemission peak. Any disorder will be manifested by the absence of structure in the diffraction pattern.

Cu 2p3/2 XPD patterns for a PE of 1045 eV from the 2.7 ML preparation before and after annealing are shown in Figure 4. In both diffraction patterns, structure is seen. An increase in intensity modulation is seen from before, figure 4(a) to after annealing, figure 4(b).

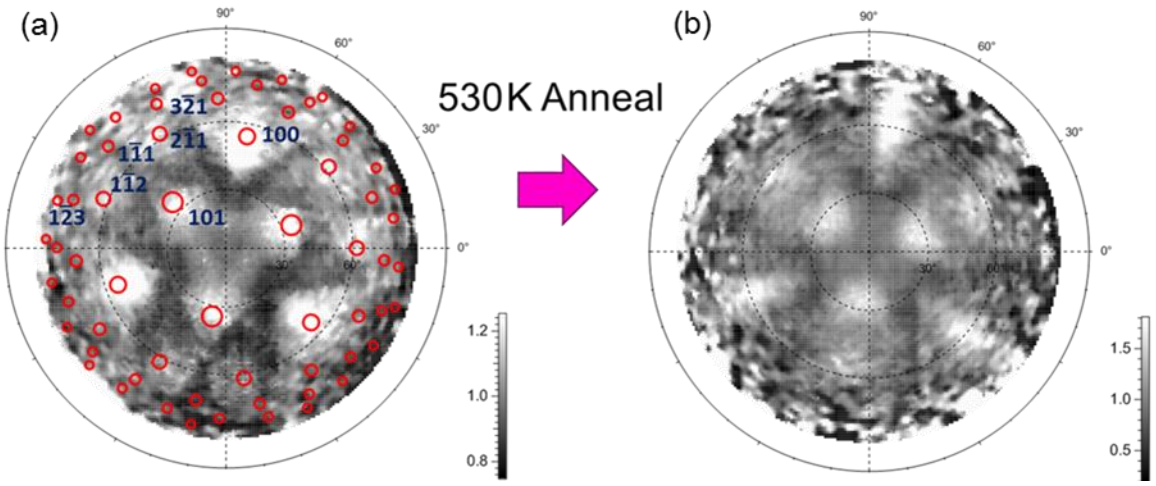

Fig. 4. XPD patterns of Cu 2p3/2 (PE 1045 eV) for the 2.7 ML preparation before (a) and after annealing (b). Crystallographic directions of an *fcc* lattice have been superposed to the 2.7 ML pattern (a); see text for further details. An increased ordering as a result of annealing can be seen in the range bar of pattern (b).

The patterns are very different from each other, thus indicating clear changes in the geometrical structure. Superposed on figure 4(a) is a pattern obtained from the stereographic projection of the *fcc* lattice, where the forward scattering peaks of the different scattering directions are depicted by circles and their intensities by the circle size. Such an approach can be regarded as a first approximation to a single-scattering calculation.[43] The model

reproduces the experimental pattern fairly well, with scattering in the ⟨110⟩, ⟨100⟩ and ⟨$\bar{1}$12⟩ directions; higher orders spots are considerably weaker or absent in the data, when compared to the model. Based on other literature studies [12, 13, 24] this suggests that the copper grows already as an alloy, or alloys, in an *fcc* structure with some disorder extending into the bulk. After annealing the pattern changes considerably, figure 4(b), however retains the principal {111} orientation of the underlying gold surface, and the main peaks grow in intensity. There are some small shifts in the ⟨110⟩ and ⟨100⟩ directions, the ⟨$\bar{1}$12⟩ essentially disappear, and a relatively intense spot appears in the ⟨22$\bar{1}$⟩ directions. The disappearance of the ⟨$\bar{1}$12⟩ spots can be due to a lowering of translational symmetry which is consistent with the geometry of the surface layers changing from an *fcc* lattice (Cu) to tetragonal (AuCu). The changes seen in the XPD pattern after annealing, figure 4(b), require further investigation, and modelling. The data here presented is dominated by forward scattering with little visible fine, secondary, structure. Perhaps this is not surprising, given the formation of a reconstruction with an averaged pseudo-periodicity larger than that of the copper film initially deposited, and some variation in the local order, as shown in figure 2(b). Consequently, the primary information obtained is an averaged lattice symmetry, whilst limited geometrical length information can be extracted from triangulation. Nevertheless, it is clear that a near surface alloy forms, the symmetry of which is no longer that of an ideal *fcc* lattice, but consistent with a distortion of the *fcc* lattice to a lower symmetry, such as a tetragonal $L1_0$. More detailed modelling of the tetragonal AuCu alloys, the related AuCu I and AuCu II phases, and other structures is being investigated.

Both observations, the growth in a preferred orientation and essentially its retention, and the structural change after annealing, given the large area of the surface covered by the moiré and other structures seen in the STM experiments, indicate that the underlying Au(111) surface is still able to influence the growth of the alloys and the interfaces.

4. Conclusions

A combined synchrotron and STM study on the growth of copper layers on the Au(111) surface and alloying on annealing has been undertaken. Preliminary data analysis show structural changes associated with the alloying process. Upon preparation, copper multilayers (*ca.* 3 ML) exhibit an overall *fcc* geometry, as determined by XPD. However, STM shows the appearance of a moiré pattern, which is ascribed to the interference of the copper and Au(111) lattices. On annealing the systems evolves into a near-surface alloy;

XPD reveals a structural change, in favour of a tetragonal geometry, and STM shows very different topographical features.

Geometrical optimization of model structures based on the experimental data and the resulting electronic structure are being pursued in order to obtain a much improved description, in the attempt to rationalize the interdiffusion of the atoms and predict the reactivity of such a system.

Acknowledgments

The Engineering and Physical Sciences Research Council (EPSRC) is acknowledged for the funding of FG (EP/M029077/1) and RM (EP/506631/1). The Paul Scherrer Institut, Villigen, Switzerland is acknowledged for provision of synchrotron radiation beamtime at the PEARL beamline of the SLS. Nicolas Bachellier, Daria Sostina and Patrick Ascher are thanked for assistance. DB thanks the Helmholtz Association Program MML for financial funding in this work. The research data supporting this publication can be accessed at https://doi.org/10.17630/a9dbff40-7bf4-4513-a28e-46af253e317e

Appendix

Additional experimental details: Survey scans using a PE of 1250 eV (for comparison with laboratory Mg Kα work) were taken along with detailed scans of the various core levels of interest and valence region. For a comparison with bulk like spectra Cu 2p, Au 4f and valence band spectra were taken with a PE of 1400 eV.

STM experimental: In-house STM measurements were performed on an Omicron variable temperature STM, operated at room temperature, in an UHV environment with a base pressure of about 1×10^{-10} mbar or lower. Topographs were acquired at room temperature in constant current mode using electrochemically etched tungsten tips. The tunneling voltage bias was applied to the tip, whereas the sample was grounded. Copper was deposited on the Au(111) crystal kept at room temperature by electrically heating a high purity copper wire (99.999%, 0.1 mm diameter), wrapped around a tantalum wire (99.999% purity, 0.25 mm diameter), to yield a deposition rate of *ca.* 0.07 ML min^{-1}. The nominal coverage in monolayer (ML) was determined by evaluating the fraction of each image covered by the features related to copper and their appearance, in combination with the calculated exposure.

References

1) S. Müller, J. Phys.: Condens. Matter **15**, R1429 (2003).
2) R. F. Zhang, X. F. Kong, H. T. Wang, S. H. Zhang, D. Legut, S. H. Sheng, S. Srinivasan, K. Rajan, and T. C. Germann, Sci. Rep. **7**, 9577 (2017).
3) W. B. Pearson, *Handbook of Lattice Spacings and Structures of Metals and Alloys*, (Pergamon Press, London, 1958).
4) C. L. Bracey, P. R. Ellis, and G. J. Hutchings, Chem. Soc. Rev. **38**, 2231 (2009).
5) M. Okada, Y. Tsuda, K. Oka, K. Kojima, W. A. Diño, A. Yoshigoe, and H. Kasai, Sci. Rep. **6**, 31101 (2016).
6) C. Cretu, and E. van der Lingen, Gold Bulletin **32**, 115 (1999).
7) V. Ozoliņš, C. Wolverton, and A. Zunger, Phys. Rev. B **57**, 6427 (1998).
8) S-. H. Wei, A. A. Mbaye, L. G. Ferreira, and A. Zunger, Phys. Rev. B **36**, 4163 (1987).
9) J. Hennig, D. Mari, and R. Schaller, Phys. Rev. B **79**, 144116 (2009).
10) Y. Feutelais, B. Legendre, and M. Guymont, Acta Mater. **47**, 2539 (1999).
11) F. Grillo, H. Früchtl, S. M. Francis and N. V. Richardson, New J. Phys. **13**, 013044 (2011).
12) L. Wang, P. Li, H. Shi, Z. Li, K. Wu, and X. Shao, J. Phys. Chem. C, **121**, 7977 (2017).
13) F. Grillo, R. Megginson, J. Christie, S. M. Francis, N. V. Richardson, and C. J. Baddeley, e-JSSNT, **16**, 163 (2018).
14) J. A. Meyer, I. D. Baikie, E. Kopatzki, and R. J. Behm, Surf. Sci. **635**, L647 (1996).
15) T. Lin, X. S. Shang, J. Adisoejoso, P. N. Liu, and N. Lin, J. Am. Chem. Soc. **135**, 3576 (2013).
16) F. Grillo, H. Früchtl, S. M. Francis, V. Mugnaini, M. Oliveros, J. Veciana, and N. V. Richardson, Nanoscale **4**, 6718 (2012).
17) R. T. Seljamae-Green, G. J. Simpson, F. Grillo, J. Greenwood, S. M. Francis, R. Schaub, J. E. Gano, H. A. Früchtl, P. Lacovig, and C. J. Baddeley Langmuir **31**, 262 (2014).
18) K. E. Wilson, and C. J. Baddeley, Surf. Sci. **629**, 102 (2014).
19) A. Delga, J. Lagoute, V. Repain, C. Chacon, Y. Girard, M. Marathe, S. Narasimhan, and S. Rousset,, Phys. Rev. B **84**, 035416 (2011).
20) A. E. Anderson, F. Grillo, C. R. Larrea, R. T. Seljamae-Green, H. A. Früchtl, and C. J. Baddeley, J. Phys. Chem. C **120**, 1049 (2016).
21) T. Trimble, L. Tang, N. Vasiljevic, N. Dimitrov, M. van Schilfgaarde, C. Friesen, C. V. Thompson, S. C. Seel, J. A. Floro, and K. Sieradzki, Phys. Rev. Lett. **95**, 166106 (2005).
22) W. Wallauer, and Th. Fauster, Surf. Sci. **331-333**, 731 (1995).

23) J. E. Macur, and R. W. Vook, Thin Solid Films **66**, 371 (1980).
24) X. Zhao, P. Liu, J. Hrbek, J. A. Rodriguez, and M. Pérez, Surf. Sci. **592**, 25 (2005).
25) J. E. Macur, and R. W. Vook, Thin Solid Films **66**, 311 (1980).
26) W. Wang, H. Shi, L. Wang, Z. Li, H. Shi, K. Wu, and X. Shao, J. Phys. Chem. C **122**, 19551 (2018).
27) M. Muntwiler, J. Zhang, R. Stania, F. Matsui, P. Oberta, U. Flechsig, L. Patthey, C. Quitmann, T. Glatzel, R. Widmer, E. Meyer, T. A. Jung, P. Aebi, R. Fasel, and T. Greber, J. Synchrotron Radiation **24**, 354 (2017).
28) Ch. Wöll, S. Chiang, R. J. Wilson, and P. H. Lippel, Phys. Rev. B **39**, 7988 (1989).
29) J. V. Barth, H. Brune, G. Ertl, and R. J. Behem, Phys. Rev. B **42**, 9307 (1990).
30) Y. Baer, P. H. Citrin, and G. K. Wertheim, Jap. J. Appl. Phys. **17**, 268 (1978).
31) J. A. Venables, G. D. T. Spiller, and M. Hanbücken, Rep. Prog. Phys. **47,** 399 (1984).
32) J. J. Yeh, and I. Lindau, Atomic Data and Nuclear Data Tables **32**, l (1985).
33) S. Tanuma, C. J. Powell, and D. R. Penn, Surf. Sci. **192**, L849 (1987).
34) J. Osterwalder, P. Aebi, R. Fasel, D. Naumovic, P. Schwaller, T. Kreutz, L. Schlapbach, T. Abukawa, S. Kono, Surf. Sci. **331-333**, 1002 (1995).
35) C. S. Fadley J. Electron Spec. Rel. Phenom. **178-179**, 2 (2010).
36) D. P. Woodrfuff, J. Electron Spec. Rel. Phenom. **178-179**, 186 (2010).
37) N. Artrith, and A. M. Kolpak, Nano Lett. **14,** 2670 (2014).
38) S. Lysgaard, J. S. G. Mýrdal, H. A. Hansen, and T. Vegge, Phys. Chem. Chem. Phys. **17**, 28270 (2015).
39) D. Liu, Y. F. Zhu, and Q. Jiang, RSC Advances. **5**, 1587 (2015).
40) D. T. Tran, and R. L. Johnston, Phys. Chem. Chem. Phys. **11**, 10340 (2009).
41) O. M. Magnussen, and R. J. Behm, J. Electroanal. Chem. **467**, 258 (1999).
42) C. Wesphal, Surf. Sci. Reports **50**, 1 (2003).
43) J. Mustre de Leon, J. J. Rehr, C. R. Natoli, C. S. Fadley, J. Osterwalder, Phys. Rev. B, **39**, 5632 (1989).

Figure Captions

Fig. 1. Schematics of the process for creating the surface alloy: (a) *ca.* 3 ML of copper (dark orange) are added to Au(111) (yellow); (b) the system is then annealed to promote atoms interdiffusion.

Fig. 2. STM images of the *ca.* 3 ML Cu/Au(111) before, (a), and after annealing, (b). (a) 35×35 nm^2, 0.6 nA, -1.1 V; (b) 35×35 nm^2, 0.7 nA, 1.1 V; inset 15×15 nm^2, 0.3 nA, 0.4 V; (c) line profiles as in (a) and (b).

Fig. 3. Cu 2p3/2 photoemission (a) and valence band (b) spectra collected at copper increasing coverage (before annealing) and after annealing. Valence band spectra have been offset for clarity.

Fig. 4. XPD patterns of Cu 2p3/2 (PE 1045 eV) for the 2.7 ML preparation before (a) and after annealing (b). Crystallographic directions of an *fcc* lattice have been superposed to the 2.7 ML pattern (a); see text for further details. An increased ordering as a result of annealing can be seen in the range bar of pattern (b).

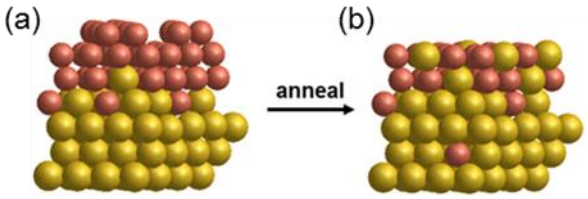

Fig.1.

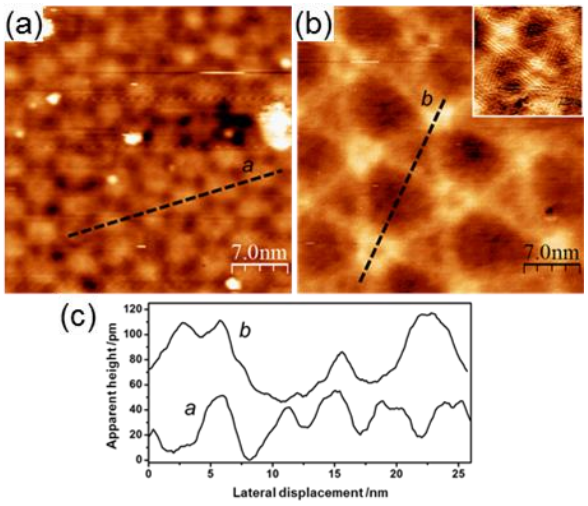
(a)
a
7.0nm
(b)
b
7.0nm
(c)
b
a
Apparent height /pm
120
100
80
60
40
20
0
0
5
10
15
20
25
Lateral displacement /nm

Fig.2.

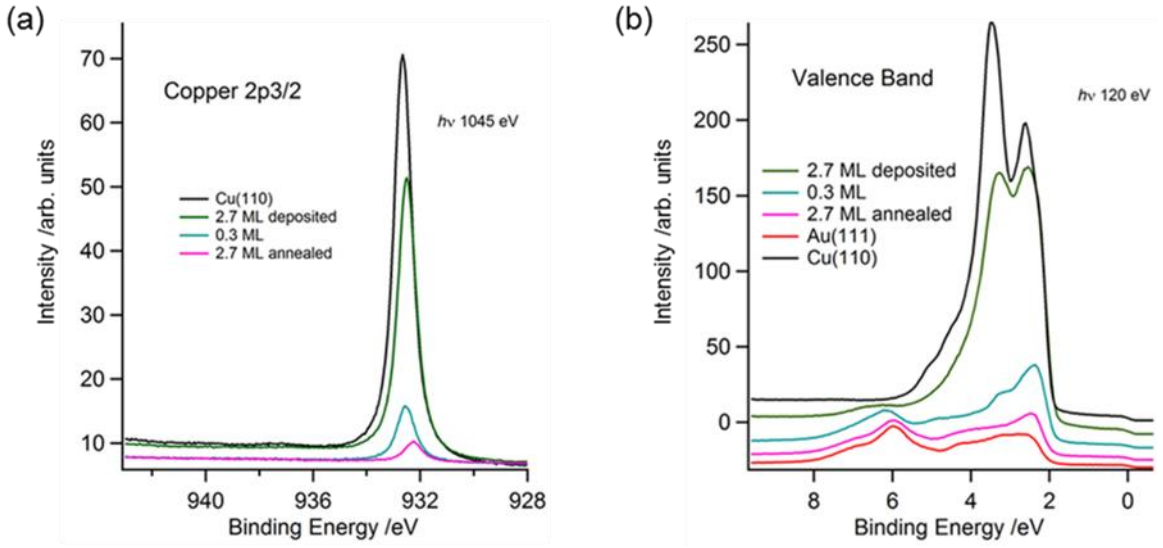
(a)
Copper 2p3/2
hν 1045 eV
Cu(110)
2.7 ML deposited
0.3 ML
2.7 ML annealed
Intensity /arb. units
Binding Energy /eV
(b)
Valence Band
hν 120 eV
2.7 ML deposited
0.3 ML
2.7 ML annealed
Au(111)
Cu(110)
Intensity /arb. units
Binding Energy /eV

Fig.3.

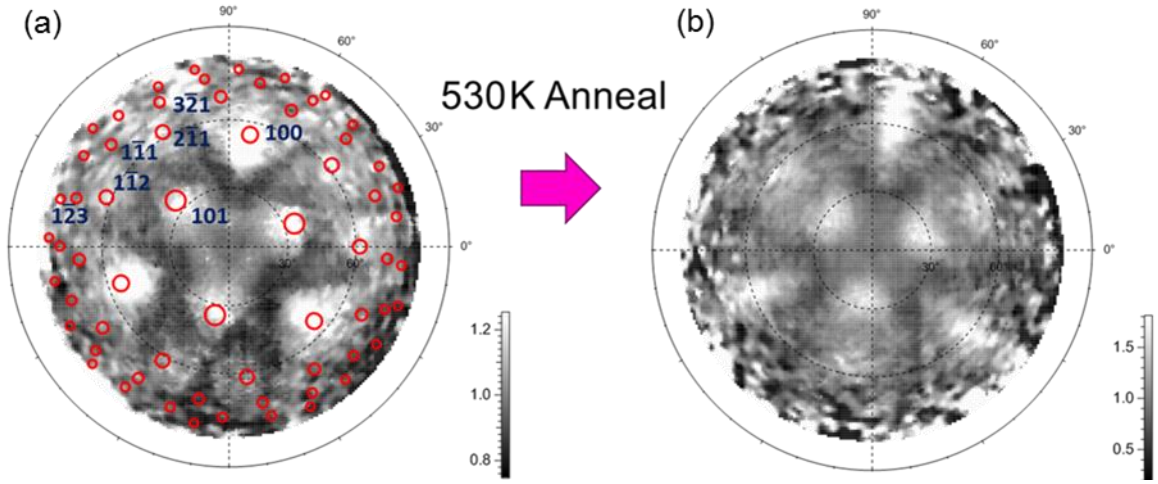
(a)
90°
60°
30°
0°
321
211
100
111
112
123
101
1.2
1.0
0.8
530K Anneal
(b)
90°
60°
30°
0°
1.5
1.0
0.5

Fig.4.